Iraqi Journal of Physics, 2025
https://doi.org/10.30723/ijp.v23i4.1388

Vol.23, No.4, PP.133-142
P-ISSN: 2070-4003
E-ISSN: 2664-5548

Synthesis and Characterization of MAPI:ZnS Color Change Detection by Ammonia Gas at Room Temperature

Amira Sabah Kataf [1*] and Fuad T. Ibrahim[1]
[1]*Department of Physics, College of Science, University of Baghdad, Baghdad, Iraq*
[*]Corresponding author: fuad.ibrahim@sc.uobaghdad.edu.iq

Abstract
The research demonstrates that perovskite methylammonium lead iodide (MAPI) can detect various hazardous and polluting chemicals, including ammonia gas (NH_3), in the environment. To enhance the sensitivity, response time, and modify the structural properties of pure MAPI, zinc sulfide (ZnS) is incorporated in three different concentrations (1, 2.5, and 5wt%). The sensitivity of these ZnS-doped samples is evaluated for detecting NH_3 and alcohol vapor. Sensors based on MAPI:ZnS composites are fabricated on writing paper samples using a solution-processing technique. Upon exposure to NH_3, MAPI undergoes a colorimetric change from black to yellow. This phenomenon is attributed to the degradation of perovskite(MAPI) halides into lead (Pb) halides through the preferential adsorption of NH_3 molecules. The structural properties were analyzed using X-ray diffraction (XRD) patterns, which revealed a slight shift in the diffraction peaks towards higher 2θ angles. Field Emission Scanning Electron Microscopy (FESEM) images displayed rod-like morphologies, with an average diameter of approximately 49 nm for pure MAPI and around 46 nm for the ZnS-doped samples.

Article Info.

Keywords:
Perovskite (MAPI) Halides, MAPI:ZnS, Paper Sensor, Ammonia Gas, Gas Sensor.

Article history:
Received: Oct. 25, 2024
Revised: Jan. 27, 2025
Accepted:Feb. 19, 2025
Published:Dec.01,2025

1. Introduction
The field of thin-film gas sensors, which are used to detect harmful and hazardous gases, is well-researched and expanding quickly because of the prospective applications and the creation of novel materials particularly nanomaterials with improved functioning. Recently, various materials with various nanostructures have been extensively employed to detect dangerous contaminants [1, 2]. Ammonia (NH_3) is a highly hazardous air pollutant, exposing workers to severe danger if exposed to it for a certain period and causing many diseases. It is preferable to detect ammonia at low levels because the gas may be present in many applications, such as refrigeration, food processing and storage, fertilizers, environmental protection, chemical technologies, and ammonia nitrogen cycle. However, the detection limit of many gas sensors depends on several factors, including operating temperature and economic manufacturing. The capacity of perovskite methylammonium lead iodide (MAPI), namely MAPbX3, to interact with gases is a desirable feature that may expand its use beyond optoelectronics to gas sensor devices. X (maybe I, Br, or Cl) plays a significant role in this interaction. Ammonia detection using some perovskite-based sensors has been described recently [3]. One of the main benefits of halide perovskite is its low-cost manufacture due to its easy fabrication via the solution approach at low temperatures [4]. Light-emitting diodes [5], lasers, photodetectors [6], solar cells [7], field-effect transistors (FETs) [8], light-emitting electrochemical cells, and many more devices employ organometallic perovskites (OMPs) as very versatile materials [9]. Current researches focus on the development of thin-film gas sensors for the precise and cost-effective detection of hazardous gases [9].

Exhaled breath analysis that can identify signs of stomach, lung, or other body part illnesses requires sensitive sensors for certain gases [10]. Modern health tracking and early illness detection using breath-exhaled biomarker analysis are of great interest

nowadays. Strong links between exhaled breath and certain illnesses have been documented in several investigations [11]. On the other hand, elevated levels of ammonia in exhaled breath, measured in ppb (~100 ppb), are indicative of the disease's early stages of pathology [12].

Zinc sulfide (ZnS) is added to the halide perovskite (MAPI) solution as one of the many methods that have been discovered over the years to increase the stability of MAPI. ZnS is a solid chemical with a cubic crystal structure and an off-white or pale-yellow tint. The Zn+ and S- ions form a particular link in the molecule ZnS. Because of its large energy gap, MAPI is a semiconductor that may be used in optoelectronic applications. The greatest energy conversion efficiency and long-term stability were attained with chemical technique. Many techniques have been developed for thin-film deposition, including spray pyrolysis[13], chemical vapor deposition (CVD)[14], sol-gel, and chemical baths [15].

In this work, a gas sensor was manufactured from MAPI to detect harmful and polluting gases in the atmosphere, to maintain the health of workers from many diseases, and to improve sensing and high selectivity; zinc sulfide was added to the pure perovskite compound. The researcher developed MAPI:ZnS thin films as sensors that revealed multiple structural, morphological and optical alterations through modifications in ZnS stoichiometry.

2. Experimental Work

The researchers synthesized MAPI and MAPI:ZnS through a series of multiple steps. The production of perovskite MAPI solution required four sequential steps which used equal molar concentrations (1:1). The solution of lead iodide in methylformamide (DMF) underwent stirring at 70°C for 30 minutes before the mixture reached room temperature. MAI solution formed through MAI dissolution in DMF while stirring the mixture at room temperature for 15 minutes. The third step involved applying the prepared PbI_2 solution onto impurity-free glass substrates, followed by heating at 140°C for 30 minutes. The substrate reached room temperature after completion of its cooling process. During the fourth step the MAI solution was heated at 100°C for one hour on the same substrate. The MAPI solution successfully settled onto glass after the cooling process. Fig. 1 shows the preparation for MAPI solution and coated films.

The preparation of doped perovskite MAPI:ZnS involved three different molar ratios that required a four-step process for the first ratio. A mixture of 10 mg ZnS and 1 mL DMF produced the ZnS solution. The researchers added PbI_2 solution to 4 mL of DMF before introducing the ZnS solution and heating it at 70°C for 30 minutes. The mixture received temperature reduction to reach room temperature. The preparation of the MAI solution involved dissolving 0.15 g of MAI material in 5 mL of DMF with stirring at room temperature for 15 minutes. The PbI2-ZnS mixture, which was prepared using the two prepared solutions, was deposited onto a clean cellulose paper substrate, which was then heated at 140°C for 30 minutes until it reached room temperature. The MAI solution received final treatment by applying it to the same substrate while heating it at 100°C for one hour. The MAPI:ZnS doped solution successfully reached its final form. The structural properties of the materials were analyzed using X-ray diffraction (XRD) with Cu-Kα radiation (λ = 0.15406 nm) under 40 kV and 30 mA, scanning the angular range of 20° to 80°. Surface morphology was examined using a Field Emission Scanning Electron Microscope (FESEM, model S-1640 HITACHI, Japan) at Tehran University, employing various magnifications and detectors. The Fourier Transform Infrared (FTIR) spectra were recorded using a SHIMADZU-8400S instrument. Optical properties were evaluated using a UV-Vis spectrophotometer (CARY 100 CONC plus

UV-Vis-NIR, split-beam optics, dual detectors) with a xenon lamp, covering the wavelength range of (300–900 nm).

Figure 1: (a)solution 1, (b) solution 2, (c) deposit solution 1, and (d) deposit solution 2.

3. Results and Discussion

3. 1. XRD Examination

The XRD patterns of the ZnS-doped MAPI and MAPI samples are displayed in Fig.2. The diffraction peaks of MAPI were observed at 2θ values of 13.34°, 34.39°, and 45.24° corresponding to the (110), (112), and (212) planes, respectively. While the peaks at 12.39°, 25.74°, 38.59° and 52.34° correspond to the (001), (111), (003), and (004) planes, respectively. These results are in line with that of a previous report [16]. When ZnS was added, the MAPI crystals underwent structural deformation. The spectra showed a minor displacement of the diffraction peaks toward higher 2θ values, which is indicative of increased structural stress and decreased interplanar space, both of which can cause lattice shrinkage [17]. There were no discernible ZnS peaks in the XRD spectra. The unit cell structure of the perovskite MAPI is distorted by the quantity of ZnS in the sample. As the amount of ZnS increases, the total cell volume of MAPI decreases. Following the addition of ZnS, the XRD peaks somewhat expanded, signifying a rise in structural flaws and a decrease in crystallite size [17, 18].

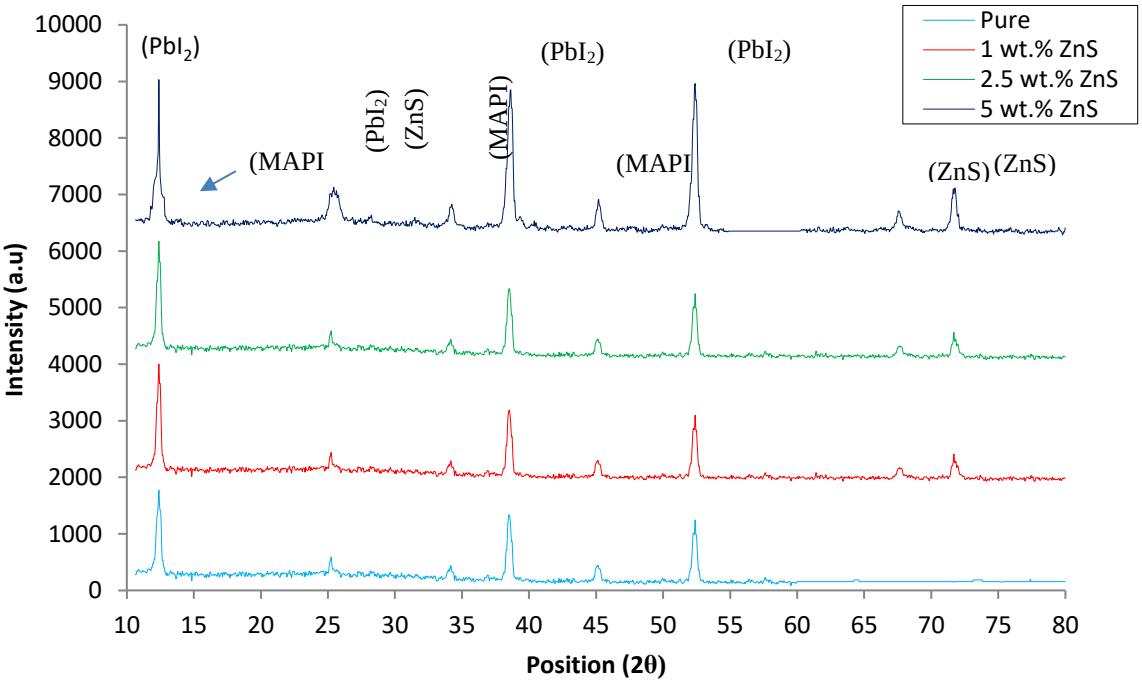

Figure 2: XRD spectra of the Pure MAPI and MAPI: ZnS thin films.

3. 2. Field Emission Scanning Electron Microscope (FESEM)

FESEM images of pure perovskite and perovskite: ZnS are presented in Fig.3, which shows ZnS in thin sheet-like structures. MAPI crystals often exhibit a dendritic morphology, allowing perovskite to grow continuously in a specific direction, ultimately resembling wires or rods [19]. The thin film of MAPI displayed an average rod diameter of approximately 49 nm. The addition of ZnS introduced porosity into the perovskite structures. As the concentration of ZnS increased, the rod-like structures began to disintegrate, transforming into irregularly shaped, smaller grains. This suggests that some of the ZnS may have formed along the growth pathway of the MAPI crystals, inhibiting further crystal development. Consequently, this resulted in increased porosity and a reduction in grain size. It is evident from Figs. 3(c)–3(d) show the grain structure changed as the ZnS content in the samples increased. When the uneven granules were eventually seen, their average diameter was 46nm.

3. 3. The FTIR Spectra

Fig.4 shows the Fourier transform Infrared (FTIR) spectroscopy spectra of pure MAPI perovskite thin films deposited on glass substrates and pure MAPI films containing varying concentrations of ZnS solution (1, 2.5, and 5 wt.%) for the wavenumber range from 500 to 4000 cm^{-1}. Table 1 presents the FTIR spectrum peaks of MAPI with different concentrations of ZnS NPs.

In the spectra of pure MAPI, a prominent peak at 3336 to 3643 cm^{-1} indicates O-H stretching. The presence of this OH peak may be attributed to moisture in the sample or the surrounding environment during the measurement [20]. Peaks at 1645 and 1537 cm^{-1} correspond to symmetric and asymmetric bending modes of NH and CH, respectively. The peak at 1031 cm^{-1} indicates C-N stretching, while the peaks at 1215 and 713 cm^{-1} are associated with $CH\text{-}NH_3$ rocking [21]. Due to the transparency of PbI_2 to infrared wavelengths, no Pb-I peak was observed in the spectrum. The optical properties of the compound, namely its ability to absorb and interact with infrared light, are considered to be the cause of this lack of a detectable peak when the compound is analyzed by infrared spectroscopy techniques like FTIR spectroscopy. The FTIR spectra of MAPI with

different concentrations of ZnS showed changes in the absorption peaks compared to that of pure MAPI. The addition of ZnS produces peak shifts in the spectra, which reveals modifications in chemical interactions between MAPI and ZnS. The spectra revealed modifications in MAPI vibrational modes because of ZnS presence, which reveals important information about material properties and interactions. The FTIR proved that there are physical interactions between MAPI and ZnS NPs. This result agrees with that of Abdelmageed et al. [21].

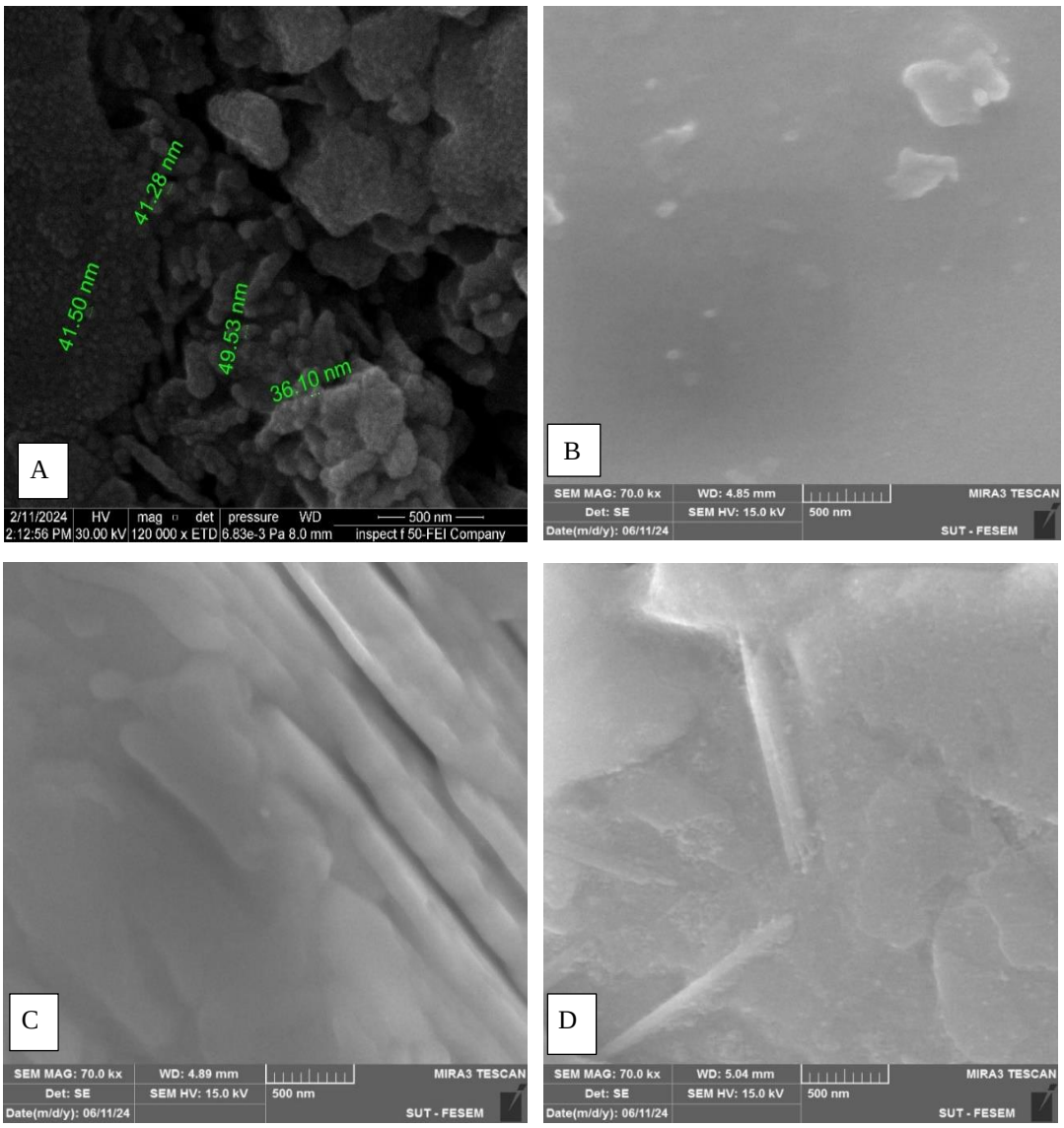

Figure 3: FESEM images of (a) pure MAPI, (b) MAPI:1wt%ZnS), (c) MAPI:2.5 wt% ZnS, and (d) MAPI:5wt% ZnS thin films.

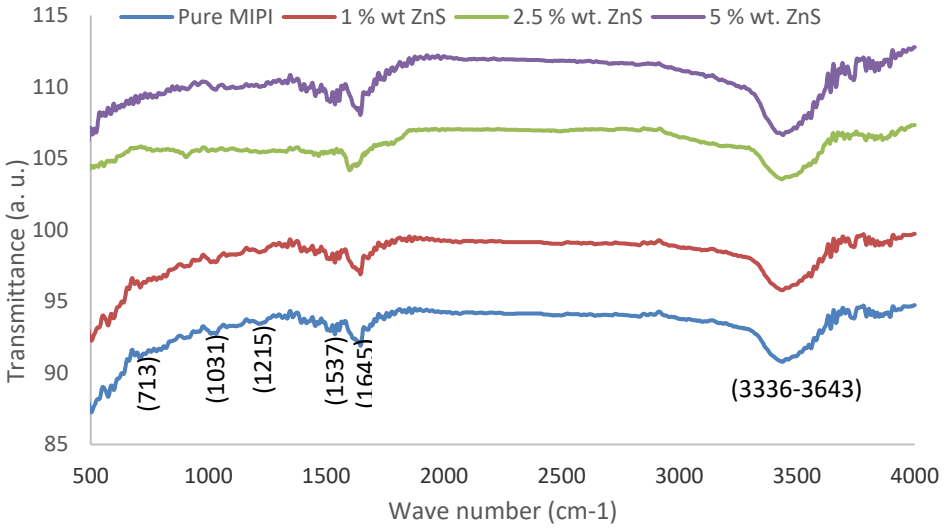

Figure 4: FTIR spectra of pure MAPI film and MAPI with different concentration of ZnS NPs.

Table 1: FTIR spectrum peaks of MAPI with different concentration of ZnS NPs.

bond type	wavenumber (cm^{-1})	vibration mode
O-H	3336-3643	stretching
NH_3	1645	symmetric bending
CH_3	1537	bending
CH^{3-}	1215	rocking
C-N	1031	stretching
NH^{3+}	713	rocking

3. 4. UV-Vis Spectrophotometry

The optical characterization was conducted using UV-Vis absorption measurements for each thin film in the wavelength range of 270 to 1100 nm. The resulting absorption spectra of pure MAI, PbI_2, and MAPI with different concentrations of ZnS nanoparticles (NPs) are presented in Fig.5. All prepared samples exhibited high absorption in the UV region. At these energy levels, donor electrons were excited to the conduction band, where absorbing a photon of known energy elevated these electrons from a lower to a higher energy state. The results demonstrated significant photon absorption by the samples in the UV region, indicating that the energy of these photons was sufficient to interact with the atoms. Furthermore, the absorbance was enhanced with an increased proportion of ZnS NPs. In contrast, the absorption values for all nanocomposites in the visible and near-infrared regions were low. The absorption rate decreased because incident photons lack adequate energy at longer wavelengths which leads to photon transmission instead of absorption [22].

The MAPI:ZnS spectra showed both position changes and absorption intensity variations due to the presence of ZnS. The MAPI film absorbance levels increased as the ZnS NPs concentration in the solution rose. The electronic structure modification, together with ZnS-MAPI interaction, causes these effects [23]. The incorporation of ZnS leads to alterations in MAPI absorbance characteristics, which indicate changes in material optical properties and interactions.

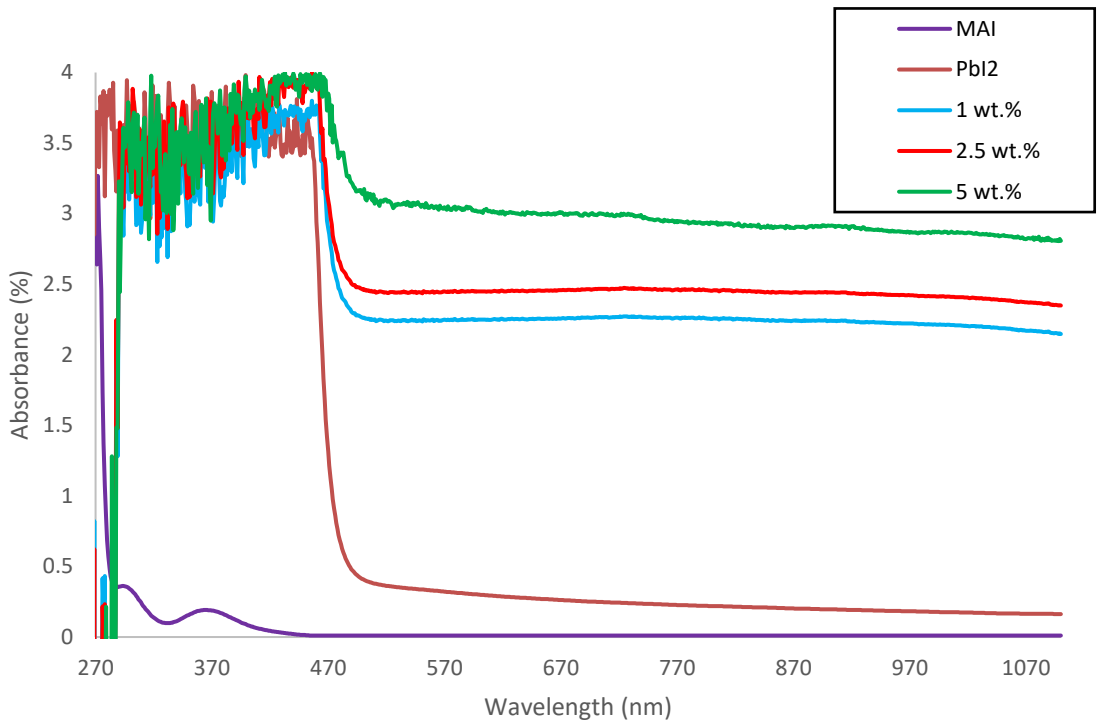

Figure 5: UV-Vis absorbance of pure MAPI film and MAPI with different concentration of ZnS NPs.

3. 5. Gas Detection Application

The gas sensing properties of the MAPI-coated paper NH_3 sensor were investigated using a simple visual color change method within a controlled gas environment in a test chamber. Upon exposure to NH_3 gas, the paper sensor changes color from black to yellow, as shown in Fig.6. This color change mechanism in the MAPI-coated paper results from the degradation of MAPI to yellow PbI_3. To support this hypothesis, a series of experiments employing structural and spectroscopic techniques were conducted to confirm that the product of the color change is indeed PbI_3.

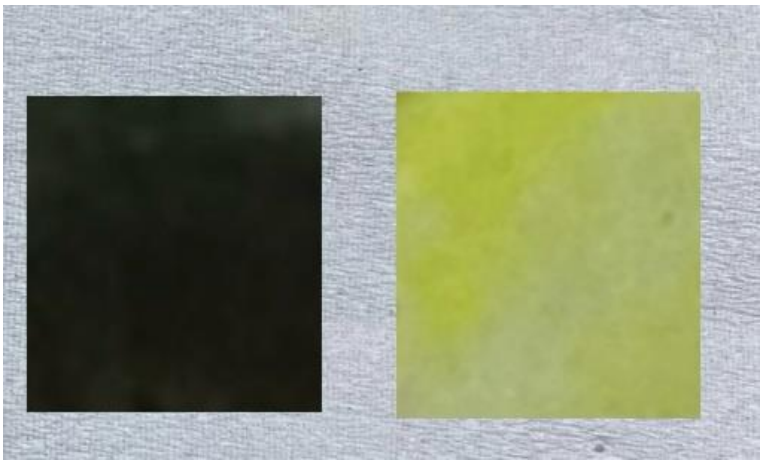

Figure 6: The MAPI visual sensor's reaction to a change in color.

Fig.7 shows the testing at room temperature of the synthesized MAPI sensors. At different concentrations of 30 ppm and 50 ppm, the sensor recognized the NH_3 gas and responded in a few seconds. Effectiveness in identifying NH_3 in the surroundings is demonstrated by this optical sensor [24]. The response time shows great dependence on

concentration such that with increase of the NH_3 concentration the response time quickly decreases. The different color map of the sensor exposed to 30 ppm and 50 ppm concentrations of NH_3 gas was recorded. The color of the sensor changes subsequently with respect to different ppm level [25].

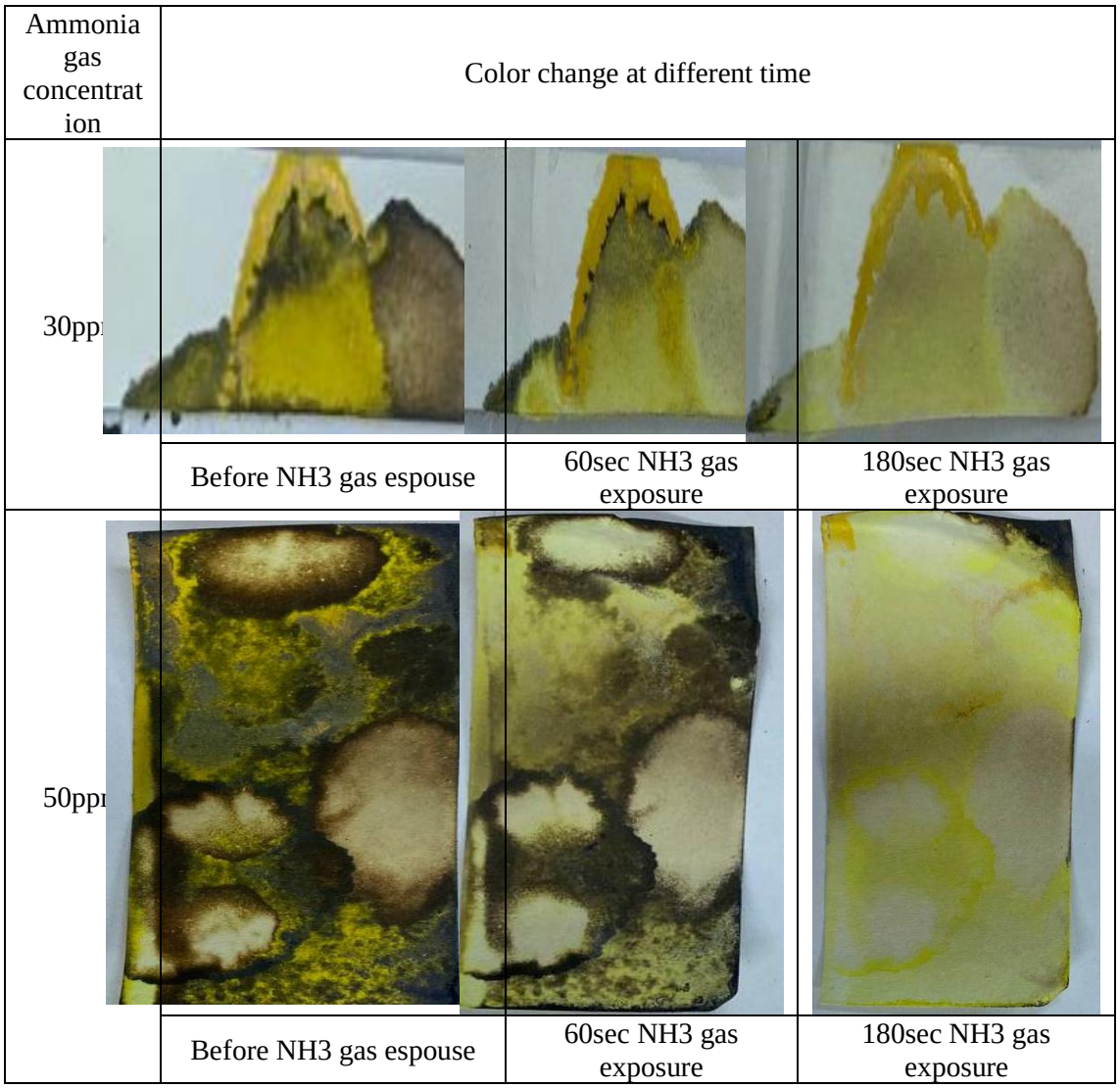

Figure 7: Color of the paper sensor at different NH3 concentrations for 60sec and 180sec time exposure.

4. Conclusions

The droplet deposition approach was used to successfully create pure MAPI and MAPI:ZnS with three distinct molar ratios. It was demonstrated that lead halide perovskites with distinct anions and cations can be utilized to develop ammonia gas sensors characterized by high sensitivity and selectivity. These sensors were fabricated on cellulose paper substrates through a solution synthesis method and can operate at room temperature. The paper-based sensors provide a straightforward approach for the selective detection of NH_3 gas. Despite some quantitative variations, the surface morphology, crystal structure, and electronic band gap remain consistent. MAPI-based sensors have exhibited superior sensitivity levels. It is suggested that the sensitivity and selectivity of lead-based perovskite halides towards NH_3 gas result from the decomposition of the material into the corresponding lead halides upon exposure to NH_3, leading to a color shift. This study illustrates that the lead-based perovskite halide family

has the potential to serve as a robust foundation for gas sensing applications at ambient temperatures.

Conflict of Interest

The authors declare that they have no conflict of interest.

References

1. S. S. Jadav, and R. Tripathi, Sensor Review, **43**, 108 (2023), https://doi.org/10.1108/SR-09-2022-0339.
2. F. T. Ibrahim, Iraqi Journal of Applied Physics **13**, 1 (2017).
3. H. J. Abdul-Ameer, M. F. AL-Hilli, and F. T. Ibrahim, Iraqi J. Sci., **64**, 630 (2023). https://doi.org/10.24996/ijs.2023.64.2.12.
4. A. S. Kataf and F. T. Ibrahim, J. Opt., **59**, 217 (2025).https://doi.org/10.1134/S1063782624602334.
5. J. Chen, S. Zhou, S. Jin, H. Li, and T. Zhai, Journal of Materials Chemistry, C **4**, 11 (2015). http://doi.org/10.1039/c5tc03417e.
6. T. Kollek et al., ACS Appl. Mater. Interfaces, **9**, 1077 (2017), https://doi.org/10.1021/acsami.6b12466.
7. F. S. Ghoreishi, V. Ahmadi, R. Poursalehi, M. SamadPour, M. B. Johansson, G. Boschloo, E. M. J. Johansson, J. Power Sources, **473**, 228492 (2020). https://doi.org/10.1016/j.jpowsour.2020.228492.
8. J. Chen, S. Zhou, S. Jin, H. Li, and T. Zhai, J. Mater. Chem., C **4**, 11 (2015). https://doi.org/10.1039/c5tc03417e.
9. S. Kalia and K. Pielichowski, *Polymer/POSS Nanocomposites and Hybrid Materials*, Springer Cham, (2018). https://doi.org/10.1007/978-3-030-02327-0.
10. C. Di Natale, R. Paolesse, E. Martinelli, and R. Capuano, Analytica Chimica Acta, **824**, 1 (2014). https://doi.org/10.1016/j.aca.2014.03.014.
11. R. Su, T. Yang, X. Zhang, N. Li, X. Zhai, and H. Chen, TrAC - Trends in Analytical Chemistry, **158**, 116823 (2023). https://doi.org/10.1016/j.trac.2022.116823.
12. S. S. Shetty, A. Jayarama, S. Bhat, Satyanarayan, I. Karunasagar, and R. Pinto, in *Materials Today: Proceedings*, **55**, 113 (2022), https://doi.org/10.1016/j.matpr.2021.12.411.
13. F. T. Ibrahim, M. A. Shahoodh, and S. Guermazi, Chem. Methodol., **7**, 871 (2023). http://doi.org/10.48309/CHEMM.2023.409731.1693.
14. C. S. Cheng, H. Gomi, and H. Sakata, Phys. Status Solidi Appl. Res., **155**, 417 (1996). https://doi.org/10.1002/pssa.2211550215.
15. Haunsbhavi, Kumar, Deva Arun Kumar, Karuppiah Mele, Paolo Aldossary, Omar M. Ubaidullah, Mohd Mahesh, H. M. Murahari, Prashantha Angadi, Basavaraj, Ceramics International.**47**, 13693 (2021), https://doi.org/10.1016/j.ceramint.2021.01.230.
16. D. Ju, T. Zhao, Y. Dang, G. Zhang, X. Hu, D. Cuia, and X. Tao J. Mater. Chem., A**5**, 21919 (2017). https://doi.org/10.1039/c7ta07413a.
17. H. Benamra, H. Saidi, A. Attaf, M. S. Aida, A. Derbali, and N. Attaf, Surfaces and Interfaces, **21**, 100645 (2020). https://doi.org/10.1016/j.surfin.2020.100645.
18. N. G. Park, Materials Today, **18**, 65 (2015), https://doi.org/10.1016/j.mattod.2014.07.007.
19. X. D. Liu, Q. Wang, Z. Q. Cheng, Y. H. Qiu, L. Zhou, and Q. Q. Wang, Mater. Lett., **206**, 75 (2017), https://doi.org/10.1016/j.matlet.2017.06.113.
20. P. V. Raleaooa, A. Roodt, G. G. Mhlongo, D. E. Motaung, R. E. Kroon, and O. M. Ntwaeaborwa, Phys. B Condens. Matter, **507**, 13 (2017). https://doi.org/10.1016/j.physb.2016.11.031.
21. G. Abdelmageed, L. Jewell, K. Hellier, L. Seymour, B. Luo, F. Bridges, J. Z. Zhang, and S. Carter, Appl. Phys. Lett., **109**, 39 (2016), https://doi.org/10.1063/1.4967840.
22. S. Tombe, G. Adam, H. Heilbrunner, D. H. Apaydin, C. Ulbricht, N. S. Sariciftci, C. J. Arendse, E. Iwuoha, and M. C. Scharber, J. Mater. Chem., C **5**, 1714 (2017). https://doi.org/10.1039/C6TC04830G.
23. J. Burschka, N. Pellet, S-Jin Moon, R. Humphry-Baker, P. Gao, M. K. Nazeeruddin, M. Grätzel, Nature, 499, 316 (2013). https://doi.org//10.1038/nature12340.
24. A. Maity, A. K. Raychaudhuri, and B. Ghosh, Sci. Rep., **9**, 1 (2019). https://doi.org/10.1038/s41598-019-43961-6
25. A. Maity, S. Mitra, C. Das, S. Siraj, A. K. Raychaudhuri, and B. Ghosh, Mater. Res. Bull., **136**, 111142 (2021), https://doi.org/10.1016/j.materresbull.2020.111142

تخليق وتوصيف يوديد الرصاص وكبريتيد الزنك ككاشف بصري لغاز الأمونيا بواسطة تغير اللون في درجة حرارة الغرفة

اميرة صباح كطاف[1] و فؤاد طارق ابراهيم[1]
[1] قسم الفيزياء، كلية العلوم، جامعة بغداد، بغداد، العراق

الخلاصة

يُظهِر البحث أن يوديد ميثيل أمونيوم الرصاص البيروفسكايت (MAPI) يمكنه الكشف عن العديد من المواد الكيميائية الخطرة والمُلوِّثة، بما في ذلك غاز الأمونيا(NH3) ، في البيئة لتعزيز الحساسية ووقت الاستجابة وتعديل الخصائص البنيوية لـ MAPI النقي، يتم دمج كبريتيد الزنك (ZnS) في ثلاثة تركيزات مختلفة (1, 2.5, and 5wt%). تم تقييم الحساسية الكهربائية لهذه العينات المحضرة بـ ZnS للكشف عن NH3وبخار الكحول. يتم تصنيع أجهزة استشعار تعتمد على مركبات MAPI: ZnS على ركائز ورقية باستخدام تقنية معالجة المحلول. عند التعرض لـNH3 ، يخضع MAPI لتغيير لوني من الأسود إلى الأصفر. تُعزى هذه الظاهرة إلى تحلل هاليدات البيروفسكايت (MAPI) إلى هاليدات الرصاص (Pb) من خلال الامتصاص التفضيلي لجزيئات NH3 .تم تحليل الخصائص البنيوية باستخدام أنماط حيود الأشعة السينية(XRD) ، والتي كشفت عن تحول طفيف في قمم الحيود نحو زوايا أعلى. أظهرت صور المجهر الإلكتروني الماسح للانبعاث الميداني (FESEM) أشكالًا تشبه السلك أو القضيب، بمتوسط قطر يبلغ حوالي 49 نانومتر لـ MAPI النقي وحوالي 46 نانومتر للعينات الممزوجة بـZnS .

الكلمات المفتاحيه: هاليدات البيروفسكايت (MAPI)، يوديد الرصاص وكبريتيد الزنك، مستشعرورقي، غاز الأمونيا، مستشعر الغاز.